Long-range enhancer activity determines *Myc* sensitivity to Notch inhibitors in T cell leukemia

Yumi Yashiro-Ohtani[a,1], Hongfang Wang[b,1], Chongzhi Zang[c], Kelly L. Arnett[d], Will Bailis[a], Yugong Ho[e], Birgit Knoechel[f], Claudia Lanauze[a], Lumena Louis[a], Katherine S. Forsyth[a], Sujun Chen[g], Yoonjie Chung[a], Jonathan Schug[e], Gerd A. Blobel[h], Stephen A. Liebhaber[e], Bradley E. Bernstein[i], Stephen C. Blacklow[d,j], Xiaole Shirley Liu[c], Jon C. Aster[b,2], and Warren S. Pear[a,2]

[a]Abramson Family Cancer Research Institute, Department of Pathology and Laboratory Medicine, and [e]Department of Genetics, and [h]Children's Hospital of Philadelphia, University of Pennsylvania, Philadelphia, PA 19104; [b]Department of Pathology, Brigham and Women's Hospital, Harvard Medical School, Boston, MA 02115; [d]Department of Biological Chemistry and Molecular Pharmacology, [f]Boston Children's Hospital, Harvard Medical School, Boston, MA 02115; [i]Broad Institute and Department of Pathology, Massachusetts General Hospital, Harvard Medical School, Boston, MA 02115; Departments of [c]Biostatistics and Computational Biology and [j]Cancer Biology, Dana–Farber Cancer Institute, Boston, MA 02115; and [g]Department of Bioinformatics, School of Life Science and Technology, Tongji University, Shanghai, China 200092

Edited by Tak W. Mak, The Campbell Family Institute for Breast Cancer Research at Princess Margaret Cancer Centre, Ontario Cancer Institute, University Health Network, Toronto, ON, Canada, and approved September 30, 2014 (received for review April 21, 2014)

Notch is needed for T-cell development and is a common oncogenic driver in T-cell acute lymphoblastic leukemia. The protooncogene c-Myc (*Myc*) is a critical target of Notch in normal and malignant pre-T cells, but how Notch regulates *Myc* is unknown. Here, we identify a distal enhancer located >1 Mb 3′ of human and murine *Myc* that binds Notch transcription complexes and physically interacts with the *Myc* proximal promoter. The Notch1 binding element in this region activates reporter genes in a Notch-dependent, cell-context–specific fashion that requires a conserved Notch complex binding site. Acute changes in Notch activation produce rapid changes in H3K27 acetylation across the entire enhancer (a region spanning >600 kb) that correlate with *Myc* expression. This broad Notch-influenced region comprises an enhancer region containing multiple domains, recognizable as discrete H3K27 acetylation peaks. Leukemia cells selected for resistance to Notch inhibitors express *Myc* despite epigenetic silencing of enhancer domains near the Notch transcription complex binding sites. Notch-independent expression of *Myc* in resistant cells is highly sensitive to inhibitors of bromodomain containing 4 (Brd4), a change in drug sensitivity that is accompanied by preferential association of the *Myc* promoter with more 3′ enhancer domains that are strongly dependent on Brd4 for function. These findings indicate that altered long-range enhancer activity can mediate resistance to targeted therapies and provide a mechanistic rationale for combined targeting of Notch and Brd4 in leukemia.

enhancer | gene regulation | chromatin | transcription | Brd4

Gain-of-function Notch1 mutations occur in >50% of human T-cell acute lymphoblastic leukemia (T-ALL) and are also frequent in murine T-ALL (1). Physiologic Notch signaling occurs when a Notch ligand on one cell engages a Notch receptor on the adjacent cell, triggering changes in the extracellular juxtamembrane region of Notch that make it susceptible to cleavage by a member of the ADAM (a disintegrin and metalloprotease domain) metalloprotease family (2). This event generates a short-lived truncated form of Notch that is proteolyzed within its transmembrane region by gamma secretase, liberating the Notch intracellular domain (NICD) from the membrane. NICD then translocates to the nucleus and forms a Notch transcription complex (NTC) with the DNA-binding protein RBPJ (recombination signal binding protein for immunoglobulin kappa J) and a Mastermind-like (MAML) factor. MAML recruits p300 and other transcriptional coactivators, leading to transcription of Notch target genes. MAML also recruits proteins leading to NICD degradation (3). The activating Notch1 mutations in T-ALL lead to either ligand-independent ADAM metalloprotease cleavage and/or diminished NICD degradation (4).

Recent studies have begun to define the function of Notch in T-ALL transcriptional regulation at the genomic level. Approximately 90% of Notch/RBPJ binding sites that mediate acute changes in gene expression are found in "super-enhancers" (5), large distal regulatory switches defined by a high content of Brd4, Med1, and H3K27ac (6, 7), a histone mark associated with active chromatin and transcription that is placed by histone acetyltransferases such as p300 (8).

The protooncogene c-Myc (*Myc*) is a particularly important direct target of Notch in normal and malignant T cells. Notch-dependent expression of *Myc* is required for normal T cells to traverse early developmental checkpoints (9, 10) and for T-ALL cells to grow and survive (11–13). Moreover, retroviral expression of Myc is sufficient to rescue some Notch-addicted T-ALL cell lines from the deleterious effects of Notch inhibition (14). Initial studies showed that NTCs bound to sites within the murine *Myc* proximal promoter (11, 13, 15), but subsequent studies showed that

Significance

The protooncogene c-Myc (Myc) is an oncogenic driver in many cancers, but is difficult to target directly with drugs. An alternative strategy is to use drugs that inhibit factors that regulate *Myc* expression. Notch drives *Myc* expression in most T-cell leukemias, but clinical trials of Notch inhibitors have been disappointing, possibly because cells emerge that express *Myc* in a Notch-independent fashion. Here we identify the genomic switches that regulate *Myc* expression in the Notch-inhibitor–sensitive and –resistant states. Our findings suggest that Notch inhibitor resistance occurs through a "switch swap" that relieves Notch dependency while increasing dependency on a different factor, bromodomain containing 4 (Brd4). These studies provide a rationale for targeting *Myc* in T cell leukemias with combinations of Notch and Brd4 inhibitors.

Author contributions: Y.Y.-O., H.W., C.Z., K.L.A., W.B., Y.H., B.K., C.L., L.L., K.S.F., Y.C., G.A.B., S.A.L., B.E.B., S.C.B., X.S.L., J.C.A., and W.S.P. designed research; Y.Y.-O., H.W., C.Z., K.L.A., W.B., Y.H., B.K., C.L., L.L., and Y.C. performed research; B.K. contributed new reagents/analytic tools; Y.Y.-O., H.W., C.Z., K.L.A., W.B., Y.H., B.K., C.L., L.L., K.S.F., S.C., Y.C., J.S., G.A.B., S.A.L., B.E.B., S.C.B., X.S.L., J.C.A., and W.S.P. analyzed data; and Y.Y.-O., H.W., C.Z., K.L.A., W.B., S.C.B., X.S.L., J.C.A., and W.S.P. wrote the paper.

The authors declare no conflict of interest.

This article is a PNAS Direct Submission.

Data deposition: The ChIP-sequencing data reported in this paper have been deposited in the Gene Expression Omnibus (GEO) database, www.ncbi.nlm.nih.gov/geo (accession no. GSE61504).

[1]Y.Y.-O. and H.W. contributed equally to this work.

[2]To whom correspondence may be addressed. Email: wpear@mail.med.upenn.edu or jaster@partners.org.

This article contains supporting information online at www.pnas.org/lookup/suppl/doi:10.1073/pnas.1407079111/-/DCSupplemental.

murine *Myc* transcription required NTC dimerization (9), which is not supported by the proximal *Myc* promoter RBPJ binding sites.

Dimeric NTCs form on sequence-paired sites (SPSs) (16), a conserved response element consisting of two head-to-head RBPJ sites separated by a spacer of 15–17 bp. Dimerization of NTCs requires cofactors of the MAML family, which stabilize the association of the NICD ankyrin repeat domain (ANK) and RBPJ, as well as several intermolecular contacts between adjacent pairs of ANK repeats in the NTC dimer. One functionally important inter-ANK contact involves the residue R1984 (formerly denoted as R1985) (17) because the Notch1 point substitution R1984A prevents NTC dimerization on SPSs, but does not affect NTC loading on monomeric RBPJ sites. In the mouse, the R1984A mutation impairs the ability of NICD1 to stimulate *Myc* expression and to induce T-ALL and T-cell development (9), pointing to the existence of at least one SPS near murine *Myc* that is critical for NTC-dependent *Myc* transcription.

We now describe studies in which whole-genome approaches were used to determine how Notch regulates *Myc* in both human and murine T-ALL cells. In both species, the critical Notch-dependent *Myc* regulatory sites are found within a large enhancer region located >1 Mb 3′ of the *Myc* transcriptional start site (TSS) containing several discrete functional domains. The major Notch complex binding sites show differential requirements for NTC dimerization in murine and human cells, an unexpected point of divergence between murine and human T-ALL. Notably, our studies indicate that the emergence of resistance to Notch inhibitors in T-ALL cells involves altered activity and use of *Myc*-associated distal enhancer domains.

Results

Identification of a Notch-Dependent Distal *Myc* Enhancer in Murine T-ALL and Primary Pre-T Cells. To identify dimeric NTC sites near *Myc*, we performed ChIP sequencing (ChIP-Seq) for Notch1 and RBPJ in the murine Notch-dependent T-ALL cell line T6E (11). Analysis of the ChIP-Seq data revealed a single prominent RBPJ/Notch1 binding site [henceforth referred to as the Notch-dependent *Myc* enhancer element (NDME)] located 1.27 Mb 3′ of the *Myc* promoter within a region with high levels of H3K4Me1, a histone mark associated with enhancers (Fig. 1*A*). Notch1 is depleted from the NDME site by short-term gamma-secretase inhibitor (GSI) treatment (Fig. 1*B*), and loading and unloading of Notch1 is associated with rapid changes in H3K27ac (Fig. S1*A*), features that characterize genomic Notch1 binding sites that dynamically regulate gene expression (5). Notch1 also bound the NDME in primary murine T-ALL cells (Fig. 1*C*) and in DN3 thymocytes (Fig. 1*D*), a stage of T-cell development marked by high levels of Notch1 activation (11). RBPJ/Notch1 binding was also observed at the previously identified *Myc* proximal promoter site (Fig. 1*A*), but these signals were substantially weaker than those seen at the NDME.

Sequence analysis of a 1-kb region centered on the RBPJ/Notch1 binding peak in the NDME revealed a single potential SPS consisting of a high-affinity RBPJ binding site (site A) oriented head-to-head with a second, lower-affinity site 15 bp away (site B) (Fig. 2*A*), an arrangement similar to that seen in other SPSs (16). Electrophoretic mobility shift assays (EMSAs) performed with an oligonucleotide containing the NDME site confirmed that it supported the loading of NTC dimers in the presence of the N-terminal portion of MAML1 and that a R1984A mutation in Notch1 suppressed dimerization on the NDME (Fig. 2*B*).

We next tested whether the NDME enhances transcription from the murine *Myc* proximal promoter in an NTC dimer-dependent fashion. Luciferase reporter constructs were designed that contained either the *Myc* promoter alone, the *Myc* promoter plus the NDME, or the *Myc* promoter plus versions of the NDME bearing mutations in either the high-affinity (site A) or low-affinity (site B) RBPJ sites of the NDME SPS element (Fig. 2*C*). T6E cells were transfected with the *Myc* promoter or the *Myc* promoter/NDME reporter together with empty vector or

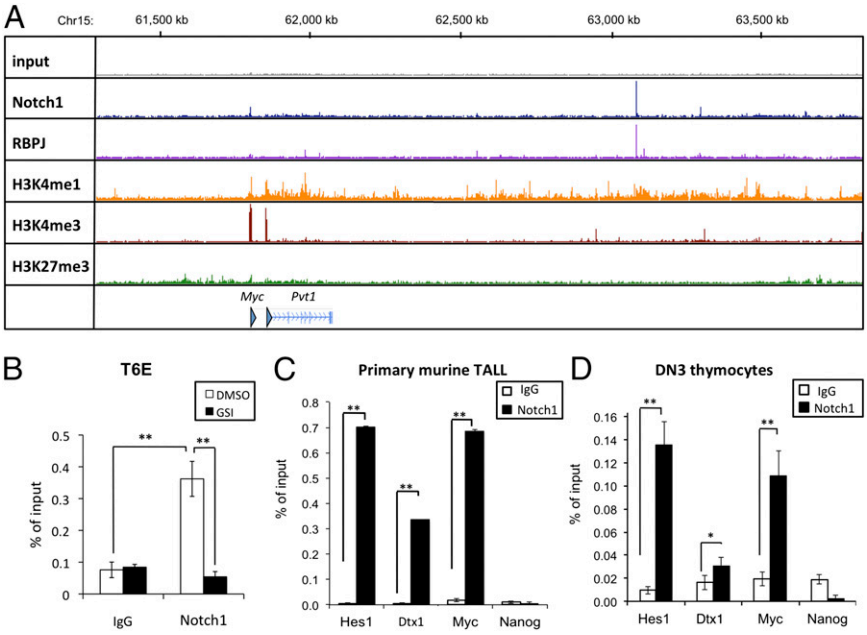

Fig. 1. Identification of a site ~1.27 Mb 3′ of the *Myc* gene body that binds RBPJ and Notch1 in normal and transformed murine pre-T cells. (*A*) ChIP-Seq read counts for Notch1, RBPJ, and H3K4me1, H3K4me3, and H3K27me3 marks in a ~2-Mb region containing *Myc*. *y* axis, aligned reads; arrowhead, TSSs. (*B*) Local ChIP for Notch1 at the 3′ *Myc* site (NDME) in the murine T-ALL cell line T6E treated with GSI or DMSO for 4 h before harvest. Nonspecific Ig was used as a control. (*C* and *D*) Local ChIP analyses of Notch1 occupancy of the binding site 3′ of *Myc* (NDME) in primary murine T-ALL cells (*C*) and DN3 thymocytes (*D*). Previously characterized Notch1 binding sites in the *Hes1* promoter and Dtx1 intron2 serve as positive controls; *Nanog* serves as a negative control. In *B–D*, data were obtained in triplicate in independent experiments; error bars correspond to the SEM. $*P < 0.01$; $**P < 0.001$.

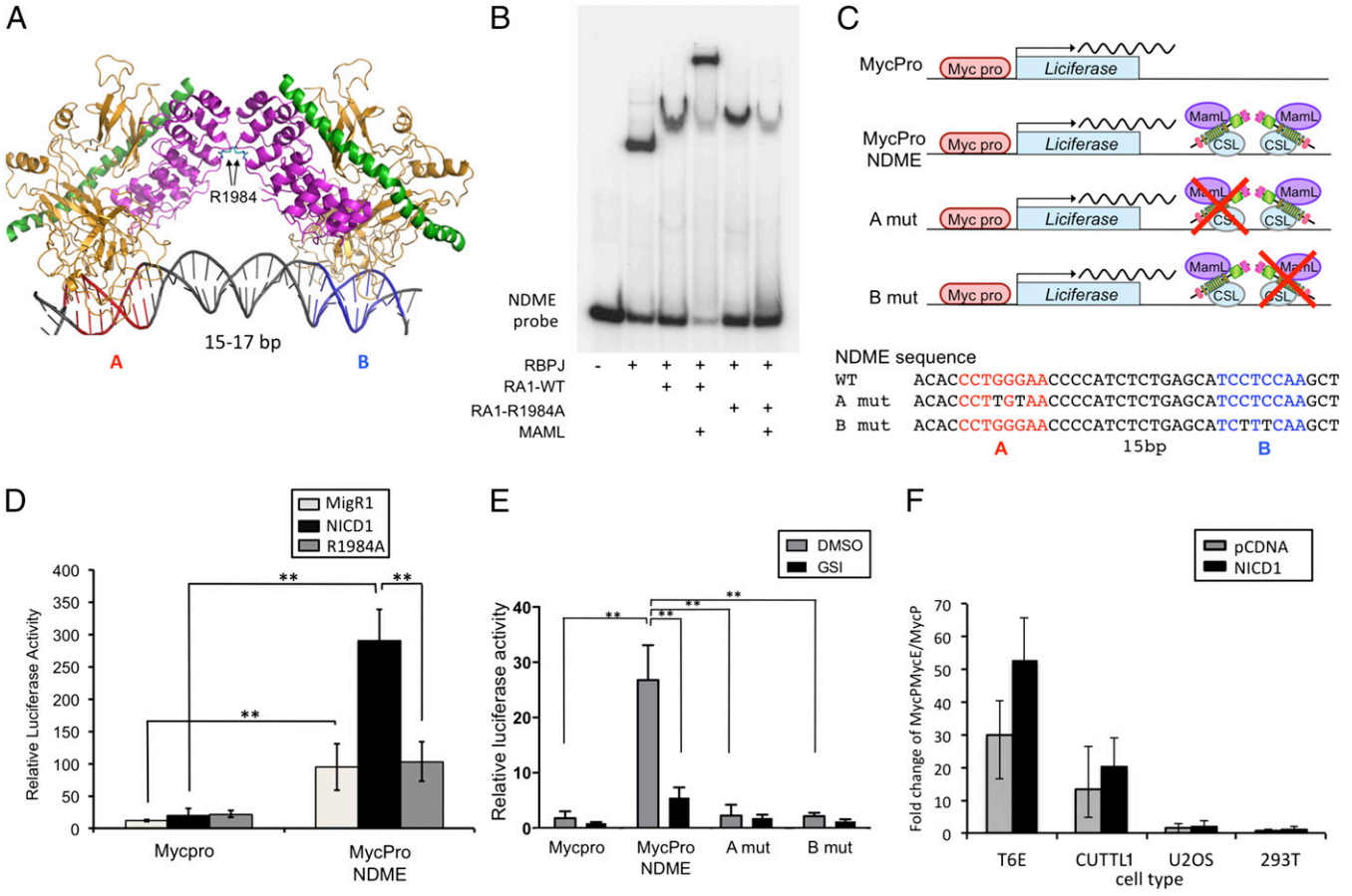

Fig. 2. The murine *Myc* 3′ enhancer contains a SPS that drives NTC dimer-dependent transcription. (*A*) Schematic of the RBPJ–Notch1–MAML NTC complex on DNA containing an SPS site. The two RBPJ motifs are designated A and B, and the critical R1984 interankyrin repeat domain contact is highlighted. See ref. 16 for details. RBPJ, gold; Notch1 RAM-ANK, purple; MAML1, green. (*B*) Assembly of dimeric NTCs on the 3′ *Myc* enhancer element. EMSA was performed with oligonucleotide probes containing the putative SPS and the indicated combinations of recombinant RBPJ, Notch1 RAM-ANKs (RA1), and N-terminal MAML1 (MAML). RA1-R1984A corresponds to the dimerization-defective Notch1 mutant. (*C*) Schematic of the luciferase reporter gene constructs including the NDME WT and mutant sequences. Note: RBPJ is denoted by its alternative name, CSL. (*D*) T6E cells were transfected with *Renilla* luciferase control (pRLTK), the indicated *Myc* firefly luciferase reporter genes, and either empty vector or vectors driving expression of WT NICD1 or NICD1 with the R1984A mutation. (*E*) Murine T-ALL T6E cells transfected with pRL-TK and one of the reporter constructs shown in *C*. Cells were cultured with DMSO or 1 μM compound E for 6 h before harvest. (*F*) Activity of the murine *Myc* enhancer reporter construct (*Myc*ProNDME) in various cell lines with and without overexpression of NICD1. In *D*–*F*, cells were harvested 48 h after transfection. Data were obtained in triplicate in independent experiments; error bars correspond to the SEM. $^{**}P < 0.001$.

vector encoding NICD1 or NICD1–R1984A. The NDME stimulated basal reporter gene activity in T6E cells, and this activity was increased further by expression of wild-type (WT) NICD1, but not by expression of the dimerization-defective R1984A mutant (Fig. 2*D*). In addition, inhibition of endogenous Notch1 with the GSI Compound E suppressed the basal activity of the NDME reporter, as did mutations in either RBPJ binding site in the NDME SPS, in line with prior data showing that loading of NTC dimers is required to activate Notch target genes with response elements containing SPSs (17) (Fig. 2*E*). Furthermore, dominant-negative mastermind (DN-MAML), a specific inhibitor of NTC function, had inhibitory effects on reporter activity comparable to those of GSI (Fig. S1*B*), consistent with the effects of GSI being mediated through Notch inhibition. In parallel studies, we noted that the NDME reporter was also active in the human T-ALL cell line CUTLL1, but not in U2OS (osteosarcoma) or HEK293T (embryonic kidney) cells (Fig. 2*F*). Collectively, these studies demonstrate that the NDME can stimulate NTC-dimer-dependent transcription in a cell-type–specific fashion.

The NDME Physically Associates with the *Myc* Promoter. To test for chromatin looping between the NDME and the *Myc* promoter, chromatin conformation capture (3C) assays were carried out in T6E cells (Fig. 3*A*). The NDME displayed an interaction frequency with the promoter that was nearly as high as that observed with sequences immediately adjacent to the promoter, whereas minimal interaction was observed between the promoter and regions between the promoter and the NDME, or sequences 40 kb 3′ of the NDME (Fig. 3*B*). To determine whether Notch signaling was required to maintain the interaction between the *Myc* promoter and the NDME, 3C analysis was performed in T6E cells cultured in the presence or absence of GSI. Although 4-h GSI treatment depleted Notch1 from the NDME (Fig. 1*B*), it did not affect the promoter–enhancer interaction (Fig. 3*C*). Thus, interaction of the *Myc* promoter and NDME is not affected by acute changes in Notch1 occupancy.

The NDME Is Conserved in Human T-ALL Cells. To determine how Notch signaling regulates *Myc* in human T-ALL cells, ChIP-Seq analysis was performed on the human T-ALL cell line CUTLL1. Analysis of the ChIP-Seq data revealed an RBPJ/Notch1 binding site associated with high levels of H3K4me1 marks located 1.43 Mb 3′ of the *Myc* promoter (Fig. 4*A*) that shares sequence homology with the murine NDME (Fig. S2). As in murine T-ALL

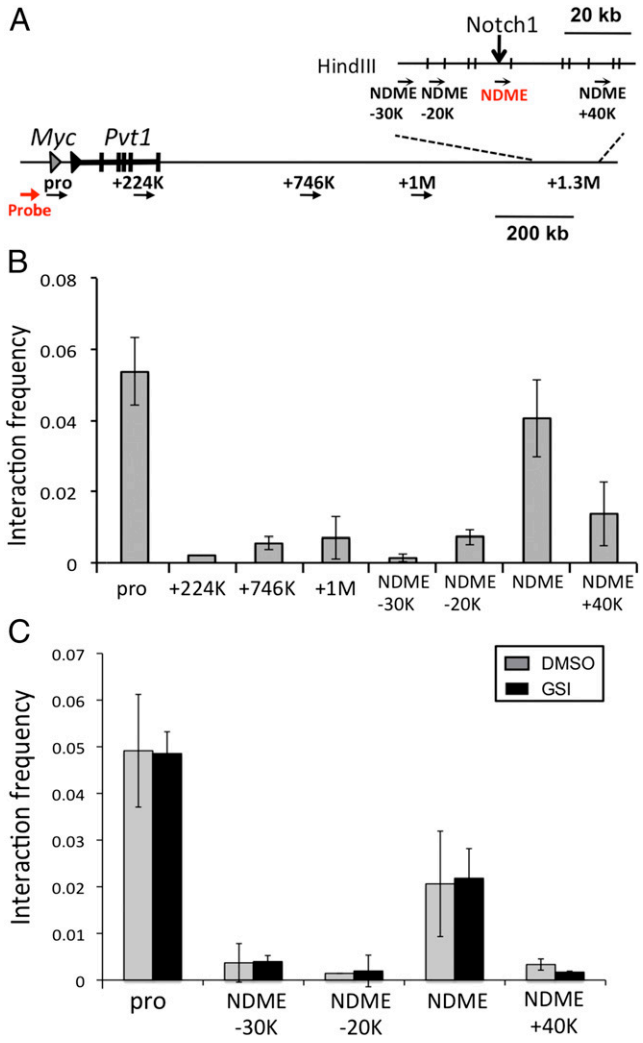

Fig. 3. Interaction of the 3′ *Myc* enhancer element and the *Myc* promoter. (*A*) Schematic of *Myc* locus and enhancer with superimposed primers used for chromosome conformation capture (3C) assay. (*B*) The 3C assay in T6E cells. Graphs show the enrichment of PCR products normalized to HindIII-digested and randomly ligated bacterial artificial chromosome (BAC) DNA spanning the region. (*C*) Short-term Notch inhibition does not affect chromatin looping. T6E cells were treated with DMSO or 1 μM GSI for 6 h. The 3C assay was performed on the *Myc* promoter and sequences 3′ of the *Myc* gene body. Positions of primers used in *B* and *C* are shown in *A*. Data were obtained in triplicate in independent experiments; error bars correspond to the SEM.

cells, 3C assays showed that the human NDME interacted with the *Myc* promoter in CUTLL1 cells (Fig. 4*B*) and that this interaction was unaffected by short-term Notch inhibition (Fig. S3). To confirm that the putative human NDME is a Notch-responsive element, luciferase reporter gene constructs containing a minimal promoter with and without the human NDME were transfected into CUTLL1 cells (Fig. 4*C*). Although the promoter-only construct was unresponsive to Notch, addition of the human NDME resulted in robust reporter activity that was sensitive to Notch inhibition, showing that this element drives Notch-dependent transcription (Fig. 4*C*).

Sequence alignment showed divergence in the SPS of the murine NDME and the analogous region of the human genome (Fig. S2). To address whether the human NDME required NTC dimerization for function, human CUTLL1 cells were transfected with the reporters described above and either WT NICD1 or NICD1–R1984A in the presence of GSI, which was added to inhibit endogenous Notch signaling. Unlike the murine NDME, the R1984A mutant stimulated transcription from the human NDME (Fig. 4*C*). In line with this observation, and in contrast to murine T-ALL cell lines (9), expression of NICD1–R1984A also rescued human Notch-addicted T-ALL lines from the effects of Notch inhibition (Fig. 4*D*). This phenotype correlated with stimulation of *Myc* expression in cells expressing either NICD1 or NICD1–R1984A (Fig. 4*E*). Thus, although the NDME is functionally conserved between man and mouse, it exhibits divergence in its dependence on NTC dimerization for *Myc* regulation.

The NDME Is Located Within a Multimodular Enhancer. Notch activation is associated with rapid increases in H3K27ac marks across the entire breadth of enhancers containing dynamic RBPJ/Notch1 binding sites, but does not alter H3K27ac in enhancers lacking RBPJ/Notch1 binding sites (Fig. S4*A*; see also ref. 5). To determine the effect of acute changes in Notch activation on H3K27 acetylation in chromatin flanking the NDME, we performed CHIP-Seq for Notch1, RBPJ, and H3K27Ac in CUTLL1 cells that were (*i*) depleted of NICD1 for 3 d with GSI or (*ii*) harvested 4 h after NICD1 activation by GSI washout. Analysis of the ChIP-Seq data revealed that the RBPJ/Notch1 site in the human NDME is located within a 3′ enhancer region of >600 kb in breadth that contains multiple domains defined by discrete H3K27ac peaks associated with Brd4 and Med1 binding (Fig. 5*A*). The major RBPJ/Notch1 binding site in this enhancer region is in the NDME (domain c), with lower-occupancy RBPJ/Notch1 binding sites also being observed in association with H3K27ac peaks at the *Myc* promoter (p) and 3′ of the NDME (domains e and f). Loading of RBPJ/Notch1 was associated with a 1.5- to 2.0-fold increase in H3K27Ac signals at the *Myc* promoter and in multiple H3K27ac peaks (domains a–j; Fig. 5*A* and Fig. S4*B*; quantified in Fig. S4 *C* and *D*), which span a region of 635 Kb. The changes H3K27ac seen in ChIP-Seq datasets were confirmed by performing local ChIP for H3K27ac in 5′ (domain c) and 3′ (domain h) portions of the 3′ *Myc* enhancer region (Fig. S5*A*), which again revealed that Notch inhibition decreased H3K27ac across the 3′ *Myc* enhancer (Fig. S5 *B* and *C*). The fold change in H3K27ac upon GSI washout (Figs. S4*D* and S5 *B* and *C*) was comparable with the fold change in *Myc* expression (Fig. S6*A*), consistent with the finding that H3K27ac is highly sensitive to changes in NTC occupancy of Notch response elements (5) (Fig. S4*A*). Thus, loading of NTCs to sites 3′ of *Myc* causes rapid increases in active chromatin marks across the entirety of the NDME-associated 3′ enhancer that correlate with stimulation of *Myc* expression.

GSI Resistance and Bromodomain Inhibitor Sensitivity Are Associated with Altered Function of Discrete Sets of Enhancer Domains. Notch-addicted human T-ALL cell lines become GSI-resistant through an epigenetic mechanism characterized by Notch-independent *Myc* expression and increased sensitivity to Brd4 inhibitors (18) (Fig. S6*B*). We therefore asked whether functional changes in the *Myc* 3′ enhancer underlie GSI resistance. Compared with GSI-sensitive T-ALL cell lines, GSI-resistant cell lines show dramatic changes in the epigenetic landscapes of the 3′ enhancer, with a loss of H3K27ac near the NDME in domains c–f, variable loss of H3K27ac in domain g, and preservation of H3K27ac marks in domains h and i and at the *Myc* promoter (Fig. 5*B*; see Fig. S6*C* for blow-up of the 3′ enhancer and Fig. S4*D* for H3K27ac quantification within specific domains). These changes in H3K27ac are closely correlated with changes in Brd4 binding among the various enhancer domains (Fig. 5*B*; quantified in Fig. S4*E*). Of note, domains h and i correspond to a Brd4-dependent enhancer region recently characterized in acute myeloid leukemia (AML) cells (19), which we henceforth term the Brd4-dependent enhancer region (BDME). The 3C assays showed

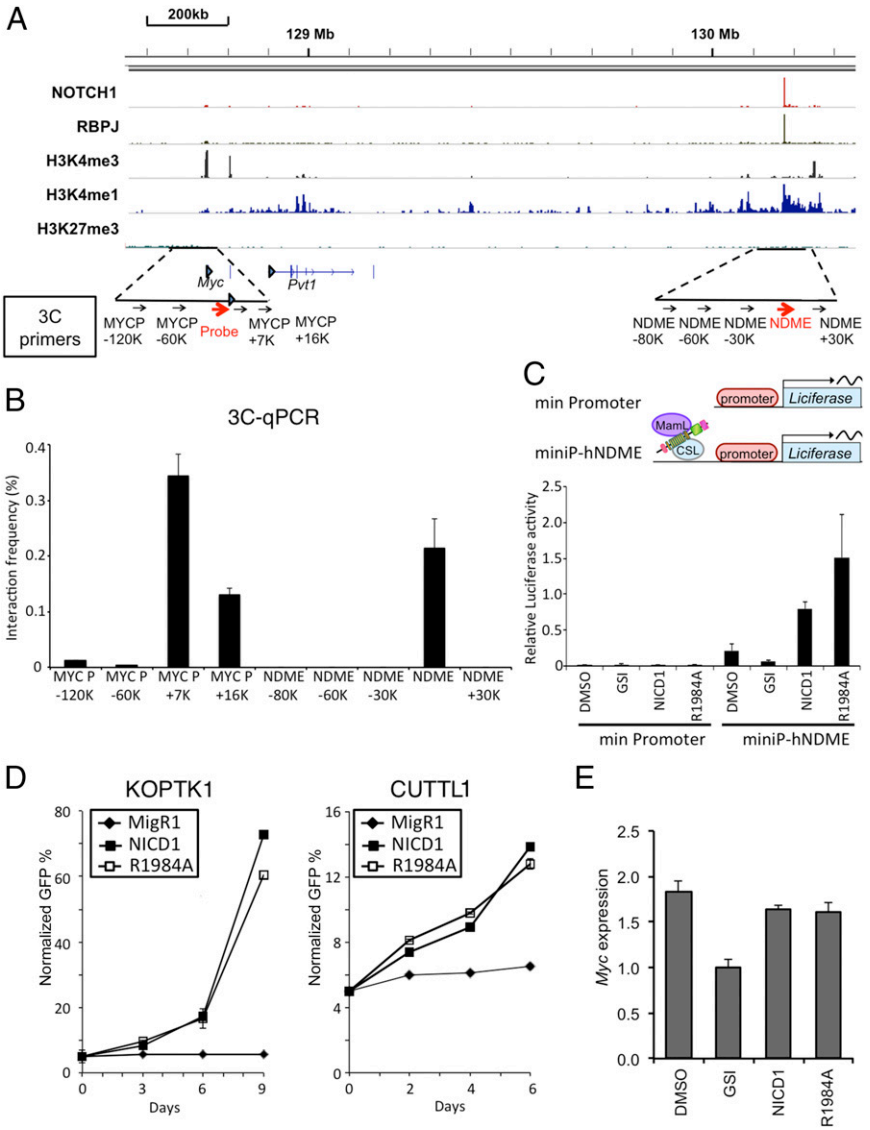

Fig. 4. Notch1 regulates human *Myc* via a 3′ enhancer element. (*A*) ChIP-Seq read counts for Notch1, RBPJ, and H3K4me1, H3K4me3, and H3K27me3 marks in a ∼2-Mb region containing human *Myc*. *y* axis, aligned sequence tags; arrowhead, TSSs. (*B*) The 3C assay in the human T-ALL cell line CUTLL1. Graphs show the enrichment of PCR product normalized to HindIII-digested, randomly ligated BAC DNA spanning the region. The arrows beneath the schematic in *A* denote the position of primers used for 3C analysis. The *Myc* promoter primer and "probe" were paired with eight primers positioned in flanking sequences to detect ligated HindIII-digestion fragments. (*C*) The human *Myc* 3′ enhancer element (NDME) stimulates transcription. (*Upper*) Schematic of the human *Myc* NDME and control firefly luciferase reporter genes. A minimal TATA promoter construct was used as a negative control. Note: RBPJ is denoted by its alternative name, CSL. (*Lower*) CUTLL1 cells were transfected with the indicated reporter genes with and without 1 μM compound E. Luciferase assays were performed 48 h later. (*D*) KOPT-K1 (*Left*) and CUTLL1 (*Right*) cells transduced with either NICD1, NICD1-R1984A, or empty plasmid were cultured in the presence of 1 μM compound E beginning 24 h after transduction. The number of GFP+ transduced cells was determined at various time points and normalized to time 0 (defined as 48 h after transduction). (*E*) *Myc* mRNA expression in CUTLL1 cells transduced as in *D*. Except for the MigR1 empty vector control cells, 1 μM compound E was added to cells 24 h after transduction. Cells were harvested for RT-PCR analysis 48 h later. In *B*–*E*, data were obtained in triplicate in independent experiments; error bars correspond to the SEM.

that the GSI-resistant state is associated with loss of NDME (domain c) interaction with the *Myc* promoter, whereas associations with the BDME (domains h and i) are maintained (Fig. 5*C*). Thus, GSI resistance is associated with alterations in the activity and higher-order structure of specific regions of the *Myc* 3′ enhancer.

Discussion

In this work, we identify a large multidomain enhancer located >1 Mb 3′ of *Myc* that appears to regulate Notch-dependent and -independent *Myc* expression in T-ALL cells. The key site mediating Notch dependence lies within a small region that we term the NDME that is conserved in position between mouse and man (20), but that shows significant divergence in RBPJ binding sites, because the murine site contains a functional paired RBPJ binding site, whereas the human site does not. Binding of Notch to chromatin in this region influences H3K27 acetylation across the entire 3′ enhancer region. Notably, T-ALL cell lines selected for resistance to Notch pathway inhibitors (18) exhibit epigenetic silencing of discrete domains within the 5′ region of the enhancer near sites of Notch binding, loss of the *Myc* promoter–NDME interaction, and preserved *Myc* promoter interaction with 3′ enhancer domains in a region termed the BDME, which was previously implicated in Brd4-dependent *Myc* expression in AML cells (19). These observations elucidate Notch-dependent and -independent

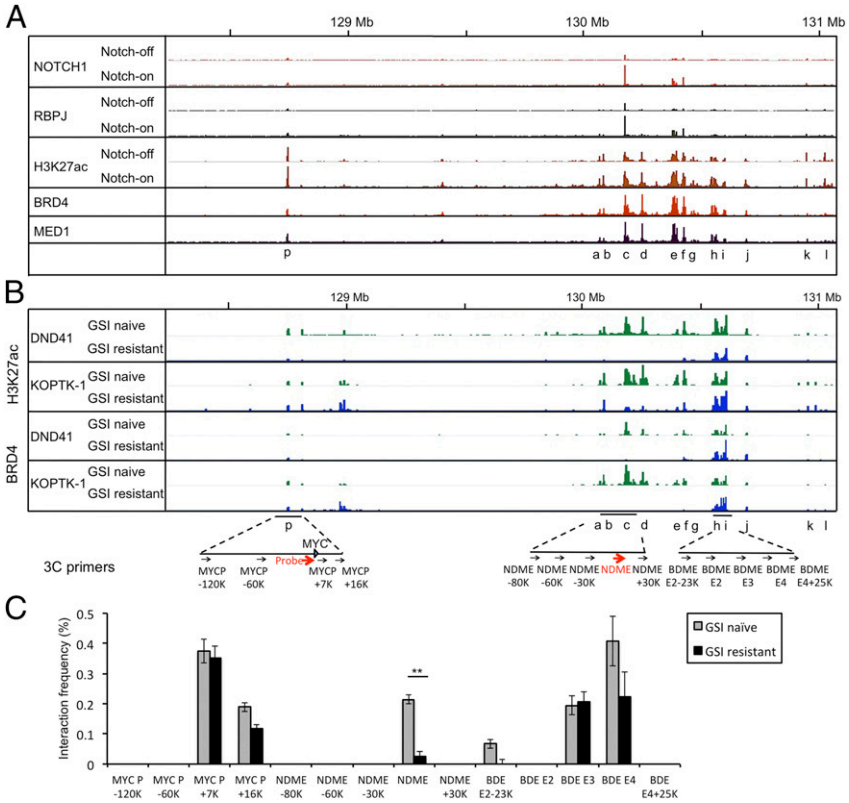

Fig. 5. Altered 3′ enhancer activity and chromatin looping in GSI-sensitive and resistant T-ALL cells. (*A*) Chromatin landscapes in human CUTLL1 cells (*i*) depleted of NICD1 by treatment with 1 μM compound E for 3 d and (*ii*) after 4 h of Notch activation by GSI washout. RBPJ, Notch1, and H3K27ac traces are shown in the Notch-on and -off states, whereas Brd4 and Med1 are shown only in the Notch-on state. H3K27ac peaks are seen at the *Myc* promoter (p) and in 3′ regions (a–l). (*B*) Chromatin landscapes in GSI-sensitive and -resistant human KOPT-K1 and DND-41 cells. H3K27ac and Brd4 traces are shown for each cell state. The positions of primers and probes used in the 3C analyses in *C* are shown below the traces. BDME, Brd4-dependent *Myc* enhancer. (*C*) The 3C analyses performed with GSI-sensitive (naïve) and GSI-resistant KOPT-K1 cells. Graphs show the enrichment of PCR products normalized to HindIII-digested, randomly ligated BAC DNA spanning the region. The 3C data were obtained in triplicate in independent experiments; error bars correspond to the SEM. $^{**}P = 0.008$ (comparing GSI-naïve with GSI-resistant samples using Student *t* test).

mechanisms of *Myc* regulation in T-ALL cells and provide insight into GSI resistance mediated by epigenetic changes.

Our findings fill in significant gaps in our understanding of the Notch–Myc signaling axis in T-ALL cells, but also raise a number of fundamental issues that remain to be resolved. First, acute changes in Notch occupancy of the NDME lead to changes in H3K27 acetylation over the full breadth of the *Myc* 3′ enhancer, a region of ∼635 kb. NTC complexes recruit p300 (3), which has been implicated in the deposition of H3K27ac marks (8), but how these marks spread in a stereotypic fashion from the site of NTC recruitment to flanking chromatin is unclear. Secondly, we identified two different chromatin states in isogenic human T-ALL cells that are sensitive to the presence or absence of Notch signals, a Notch-on state dominated by *Myc* regulation through the NDME and a Notch-off state dominated by *Myc* regulation through the BDME. Single-cell cloning assays suggest that a small fraction of Notch-mutated T-ALL cells are in the GSI-resistant state before exposure of bulk cell populations to drug (18), but how individual cells shift between the GSI-sensitive and -resistant chromatin states is unknown. Third, short-term withdrawal of Notch binding did not affect looping of the NDME to the *Myc* promoter, whereas NDME functional activity and looping were both lost in cells selected for GSI resistance. Because the NDME remains in proximity to the *Myc* promoter during acute inhibition, other factors must be required to maintain transcription, as has been described for SATB1 during Th2 cell activation (21). Finally, because NTCs (22) and Brd4 (23) appear to regulate transcription by recruiting different multiprotein complexes and therefore might be expected to complement one another, it is unclear how high levels of activated Notch lower the requirement for Brd4, a conclusion drawn from both drug-sensitivity and shRNA-knockdown studies (18).

Our work adds to emerging themes in an increasingly complex picture of *Myc* regulation by long-range enhancer elements. Cell-type–specific *Myc* enhancers have now been described in colorectal cancer (24, 25), T-ALL (this work), AML (19), and other hematopoietic neoplasms (7). When tested as isolated DNA fragments in reporter constructs, these elements drive transcription in a cell-context–restricted fashion, a phenomenon we observed for the NDME in T-ALL cells that is also true of the BDME in AML cells (19) and for other *Myc* enhancers in colorectal cancer (24, 25). This characteristic presumably stems from cell-type–specific cofactors that have yet to be identified. Moreover, the potential for coregulation of *Myc* by multiple enhancer inputs provides for an additional level of complexity. We observed interaction of the *Myc* promoter in "Notch-on" T-ALL cells with discrete enhancer domains located in the NDME and BDME, a finding similar to the cosynapsis of two Wnt-dependent enhancer elements located 5′ and 3′ of the *Myc* gene body with the *Myc* promoter in colorectal cancer cells (25). Finally, Notch-mediated *Myc* activation is proposed to be an important event in other human tumors besides T-ALL with Notch gain-of-function mutations—including marginal zone lymphoma (26, 27), mantle cell lymphoma (28), and breast cancer (29)—and it remains to be determined whether Notch uses the NDME in each of these

varied tumor types and, if so, whether it does so together with other enhancers that interact with the *Myc* promoter.

These complexities may represent an opportunity for targeting *Myc* in cancer. It appears that *Myc* expression in T-ALL is regulated by at least two epigenetic states in which *Myc* expression is GSI-sensitive or Brd4 inhibitor-sensitive, respectively, suggesting that emergence of drug resistance to either agent may be prevented by cotreatment strategies. This cooperative regulation is supported by preclinical studies of human T-ALLs, which respond better to GSI/Brd4 inhibitor combinations than to either drug alone (18). Our findings bolster the mechanistic rationale for cotargeting of Notch and Brd4 in T-ALL and suggest that this drug combination merits study in other preclinical models of Notch-driven cancers.

Materials and Methods

Cells. Primary murine T-ALL cells were obtained from mice that received $Kras^{G12D}$ bone marrow transduced with the Notch1 L1601P mutant (30); GFP-positive $CD4^+CD8^+$ T-ALL cells were isolated from the spleen by sorting. DN3 cells from $Rag2^{-/-}$ mice were negatively selected with biotinylated antibodies against NK1.1, CD11b, CD11c, B220, Ter119, and CD44 with streptavidin beads (Miltenyi Biotec) and confirmed to be >98% pure. Murine and human T-ALL cell lines were cultured in RPMI medium 1640 (Invitrogen) supplemented with 10% FBS, 2 mM L-glutamine, 100 IU per 100 μg per mL penicillin/streptomycin, 1 mM sodium pyruvate, and 5 μM 2-mercaptoethanol. In GSI washout studies, CUTLL1 cells were treated with the GSI compound E (1 μM) (31) for various periods of time, washed, and then replated in either 1 μM GSI (washout control) or in DMSO for 4 h (washout). GSI-resistant KOPT-K1 and DND41 cells were as described (17). U2OS and 293T cells were cultured in DMEM (Invitrogen) supplemented with 10% FBS, 2 mM L-glutamine, and 100 IU per 100 μg per mL penicillin/streptomycin.

ChIP Assays. ChIP was performed as described (32). Briefly, chromatin samples prepared from fixed cells were immunoprecipitated with rabbit IgG (no. sc-3888, Santa Cruz Biotechnology), anti-Notch1 antibodies (33), or anti-H3K27Ac antibody (no. ab4729, Abcam). Genomic DNA was quantified by real-time PCR with primers (Table S1) flanking RBPJ binding sites or H3K27ac peaks located in the NDME or BDME (in human). Positive controls for Notch1 ChIP were prepared from the *Hes1* promoter and *Dtx1* intron2, and ChIP for *Nanog* was used as an internal negative control. Enrichment was measured by using the absolute standard curve method. The DNA quantity recovered from each ChIP sample is expressed relative to input DNA.

ChIP-Seq. ChIP was performed as described above, and libraries were constructed per the NEB NEXT kit (5, 34). High-throughput sequencing was performed by using the Illumina Genome Analyzer II. Reads were mapped to human genome hg19 or mouse genome mm9. ChIP-Seq data were processed as described (5, 34). All binding signals were normalized to reads per kilobase per million mapped reads. High-confidence peaks were defined by ChIP enrichment of greater than or equal to threefold and a false discovery rate (FDR) of <0.01. The FDR was determined by running the same peak calling analysis on a randomly selected subset of the input ChIP-Seq data. ChIP-Seq data (accession no. GSE61504) are available through the Gene Expression Omnibus database (www.ncbi.nlm.nih.gov/geo/). Other ChIP-Seq analyses were conducted using published datasets (5, 18) (accession nos. GSE54380, GSE51800, and GSE29600).

ChIP-Seq Data Analysis. ChIP-Seq data were aligned to either human genome build hg19 or mouse genome build mm9, and uniquely mapped, nonredundant reads were retained. Genomic wiggle traces were generated by using MACS (Version 1.4) (35), normalized by the total nonredundant read count of each sample, and displayed using IGV Browser. H3K27ac peaks were identified in T-ALL Notch-on datasets by using SICER (Version 1.1) with default parameters (36). In the *Myc* 3′ enhancer region, individual H3K27ac peaks were additionally filtered with a SICER island score threshold of 3,000. Comparisons of H3K27ac levels in the Notch-on/Notch-sensitive state and Notch-off/Notch-resistant state were performed by using SICER differential comparison function (36). *P* values were reported after Benjamini–Hochberg correction for multiple-hypothesis testing over all H3K27ac peaks in the genome.

Quantitative RT-PCR. RNA was extracted with the QIAGEN RNeasy Mini Kit. cDNA was synthesized from RNA with the SuperScript III kit (Invitrogen). Transcripts were amplified with Sybr Green PCR Master Mix (ABI), and quantitative PCR was performed on an ABI ViiA 7 real-time PCR System. Primers are provided in Table S1.

EMSA. EMSA was performed as described (17). Recombinant RBPJ (residues 9–435), WT or R1984A mutant Notch1 (residues 1,761–2,127), and MAML1 (residues 13–74) were expressed and purified as described (37). In the current release of the human genome, the key arginine residue at the dimerization interface of the Notch1 ankyrin repeats (formerly referred to as R1985 in prior publications) (9, 17) is R1984. Oligonucleotides used to create probes for EMSAs are listed in Table S1.

Luciferase Reporter Gene Assay. Murine *Myc* promoter (Mycpro) constructs containing DNA corresponding to −1,137 to +516 bp from the *Myc* TSS were cloned into the pGL3 vector (Promega). The murine or human *Myc* NDME, corresponding to positions chr15:63,087,071–63,087,595 (525 bp) and hg19 chr8:130,180,217–130,180,629 (413 bp) in the murine and human genomes, respectively, were cloned into pGL3 Mycpro or the pGL3-SV40 vector. Mutagenesis was performed with the QuikChange Site-Directed Mutagenesis Kit (Agilent Technologies). T6E or CUTLL1 cells were transfected with 200 ng of the indicated reporter constructs, 50 ng of pRL-TK, and 200 ng of pcDNA–NICD1, pcDNA–NICD1–R1984A, pcDNA–DN–MAML, or empty vector with Lipofectamine LTX-plus reagent (Life Technologies). The 293T and U2OS cells were plated in triplicate and transfected with 50 ng of the indicated promoter/reporter constructs, 10 ng of pRL-TK, and 10 ng of pcDNA–NICD1 or vector control by using FuGENE 6 (Promega). For the U2OS and 293T cell assays, a Hes1 reporter was used as a positive control (33). The relative *Myc* enhancer activity (MycProNDME) was determined relative to the *Myc* promoter (MycPro) activity. Luciferase assays were performed as described (38). Firefly luciferase values were normalized with the *Renilla* luciferase internal control and expressed relative to activities obtained with promoter-only plasmids. The values are averages of three independent experiments; error bars show the SEM.

Chromatin Conformation Capture Assay. Assay was performed as described (39). Briefly, cells cross-linked with 1% formaldehyde at room temperature for 10 min were quenched with glycine, lysed, and treated with HindIII followed by T4 ligase. Ligated products were quantified in triplicate by TaqMan real-time PCR. Probes and primers were designed by using Primers3 software. Control 3C template was generated by using two bacterial artificial chromosomes (BACs) that together encompass *Myc* and the relevant flanking regions (listed in Table S1). Equimolar amounts of the two BAC clones were digested with HindIII and ligated. PCR DNA fragments obtained from BAC 3C DNA were purified and adjusted to a concentration of 1 nM, and then used to generate PCR standard curves to which all 3C PCR products were normalized. Ct values are within the linear range over at least one order of magnitude (Figs. S7 and S8). Probe, primer sequences, and BAC clones are listed in Table S1.

ACKNOWLEDGMENTS. We thank Junwei Shi and Chris Vakoc (Cold Spring Harbor Laboratory) for sharing information prior to publication. The University of Pennsylvania Mouse Husbandry Core (University Laboratory Animal Resources), the Abramson Cancer Center Flow Cytometry Core (P30-CA016520), the Abramson Family Cancer Research Institute Core, the Functional Genomics Core, and the NIH/National Institute of Diabetes and Digestive and Kidney Diseases P30 Center for Molecular Studies in Digestive and Liver Diseases (P30-DK050306), contributed to this study. This work was supported by a Leukemia and Lymphoma Society fellowship (to C.Z.); Fellowships T32HD007516 and 1F31CA165813 (to W.B.); St. Baldrick's Fellowship T32HL007574 (to B.K.); National Institutes of Health Grants P01 CA119070 (to J.C.A., W.S.P., S.C.B., and X.S.L.), R01AI047833 (to W.S.P.), R01HD25147 (to S.A.L.), and ENCODE U54 HG004570 (to B.E.B.); and a Leukemia and Lymphoma Society Specialized Center of Research grant (to J.C.A. and B.E.B.).

1. Aster JC, Blacklow SC, Pear WS (2011) Notch signalling in T-cell lymphoblastic leukaemia/lymphoma and other haematological malignancies. *J Pathol* 223(2): 262–273.
2. Hori K, Sen A, Artavanis-Tsakonas S (2013) Notch signaling at a glance. *J Cell Sci* 126(Pt 10):2135–2140.
3. Fryer CJ, Lamar E, Turbachova I, Kintner C, Jones KA (2002) Mastermind mediates chromatin-specific transcription and turnover of the Notch enhancer complex. *Genes Dev* 16(11):1397–1411.
4. Tzoneva G, Ferrando AA (2012) Recent advances on NOTCH signaling in T-ALL. *Curr Top Microbiol Immunol* 360:163–182.

5. Wang H, et al. (2014) NOTCH1-RBPJ complexes drive target gene expression through dynamic interactions with superenhancers. *Proc Natl Acad Sci USA* 111(2):705–710.
6. Whyte WA, et al. (2013) Master transcription factors and mediator establish super-enhancers at key cell identity genes. *Cell* 153(2):307–319.
7. Lovén J, et al. (2013) Selective inhibition of tumor oncogenes by disruption of super-enhancers. *Cell* 153(2):320–334.
8. Jin Q, et al. (2011) Distinct roles of GCN5/PCAF-mediated H3K9ac and CBP/p300-mediated H3K18/27ac in nuclear receptor transactivation. *EMBO J* 30(2):249–262.
9. Liu H, et al. (2010) Notch dimerization is required for leukemogenesis and T-cell development. *Genes Dev* 24(21):2395–2407.
10. Li X, Gounari F, Protopopov A, Khazaie K, von Boehmer H (2008) Oncogenesis of T-ALL and nonmalignant consequences of overexpressing intracellular NOTCH1. *J Exp Med* 205(12):2851–2861.
11. Weng AP, et al. (2006) c-Myc is an important direct target of Notch1 in T-cell acute lymphoblastic leukemia/lymphoma. *Genes Dev* 20(15):2096–2109.
12. Sharma VM, et al. (2006) Notch1 contributes to mouse T-cell leukemia by directly inducing the expression of c-myc. *Mol Cell Biol* 26(21):8022–8031.
13. Palomero T, et al. (2006) NOTCH1 directly regulates c-MYC and activates a feed-forward-loop transcriptional network promoting leukemic cell growth. *Proc Natl Acad Sci USA* 103(48):18261–18266.
14. Chan SM, Weng AP, Tibshirani R, Aster JC, Utz PJ (2007) Notch signals positively regulate activity of the mTOR pathway in T-cell acute lymphoblastic leukemia. *Blood* 110(1):278–286.
15. Klinakis A, et al. (2006) Myc is a Notch1 transcriptional target and a requisite for Notch1-induced mammary tumorigenesis in mice. *Proc Natl Acad Sci USA* 103(24): 9262–9267.
16. Arnett KL, et al. (2010) Structural and mechanistic insights into cooperative assembly of dimeric Notch transcription complexes. *Nat Struct Mol Biol* 17(11):1312–1317.
17. Nam Y, Sliz P, Pear WS, Aster JC, Blacklow SC (2007) Cooperative assembly of higher-order Notch complexes functions as a switch to induce transcription. *Proc Natl Acad Sci USA* 104(7):2103–2108.
18. Knoechel B, et al. (2014) An epigenetic mechanism of resistance to targeted therapy in T cell acute lymphoblastic leukemia. *Nat Genet* 46(4):364–370.
19. Shi J, et al. (2013) Role of SWI/SNF in acute leukemia maintenance and enhancer-mediated Myc regulation. *Genes Dev* 27(24):2648–2662.
20. Geimer Le Lay AS, et al. (2014) The tumor suppressor Ikaros shapes the repertoire of notch target genes in T cells. *Sci Signal* 7(317):ra28.
21. Cai S, Lee CC, Kohwi-Shigematsu T (2006) SATB1 packages densely looped, transcriptionally active chromatin for coordinated expression of cytokine genes. *Nat Genet* 38(11):1278–1288.
22. Yatim A, et al. (2012) NOTCH1 nuclear interactome reveals key regulators of its transcriptional activity and oncogenic function. *Mol Cell* 48(3):445–458.
23. Rahman S, et al. (2011) The Brd4 extraterminal domain confers transcription activation independent of pTEFb by recruiting multiple proteins, including NSD3. *Mol Cell Biol* 31(13):2641–2652.
24. Tuupanen S, et al. (2009) The common colorectal cancer predisposition SNP rs6983267 at chromosome 8q24 confers potential to enhanced Wnt signaling. *Nat Genet* 41(8): 885–890.
25. Yochum GS, Sherrick CM, Macpartlin M, Goodman RH (2010) A beta-catenin/TCF-coordinated chromatin loop at MYC integrates 5′ and 3′ Wnt responsive enhancers. *Proc Natl Acad Sci USA* 107(1):145–150.
26. Rossi D, et al. (2012) The coding genome of splenic marginal zone lymphoma: Activation of NOTCH2 and other pathways regulating marginal zone development. *J Exp Med* 209(9):1537–1551.
27. Kiel MJ, et al. (2012) Whole-genome sequencing identifies recurrent somatic NOTCH2 mutations in splenic marginal zone lymphoma. *J Exp Med* 209(9):1553–1565.
28. Kridel R, et al. (2012) Whole transcriptome sequencing reveals recurrent NOTCH1 mutations in mantle cell lymphoma. *Blood* 119(9):1963–1971.
29. Robinson DR, et al. (2011) Functionally recurrent rearrangements of the MAST kinase and Notch gene families in breast cancer. *Nat Med* 17(12):1646–1651.
30. Chiang MY, et al. (2008) Leukemia-associated NOTCH1 alleles are weak tumor initiators but accelerate K-ras-initiated leukemia. *J Clin Invest* 118(9):3181–3194.
31. Shelton CC, et al. (2009) Modulation of gamma-secretase specificity using small molecule allosteric inhibitors. *Proc Natl Acad Sci USA* 106(48):20228–20233.
32. Yashiro-Ohtani Y, et al. (2009) Pre-TCR signaling inactivates Notch1 transcription by antagonizing E2A. *Genes Dev* 23(14):1665–1676.
33. Aster JC, et al. (2000) Essential roles for ankyrin repeat and transactivation domains in induction of T-cell leukemia by notch1. *Mol Cell Biol* 20(20):7505–7515.
34. Wang H, et al. (2011) Genome-wide analysis reveals conserved and divergent features of Notch1/RBPJ binding in human and murine T-lymphoblastic leukemia cells. *Proc Natl Acad Sci USA* 108(36):14908–14913.
35. Zhang Y, et al. (2008) Model-based analysis of ChIP-Seq (MACS). *Genome Biol* 9(9): R137.
36. Zang C, et al. (2009) A clustering approach for identification of enriched domains from histone modification ChIP-Seq data. *Bioinformatics* 25(15):1952–1958.
37. Nam Y, Sliz P, Song L, Aster JC, Blacklow SC (2006) Structural basis for cooperativity in recruitment of MAML coactivators to Notch transcription complexes. *Cell* 124(5): 973–983.
38. Bailis W, et al. (2013) Notch simultaneously orchestrates multiple helper T cell programs independently of cytokine signals. *Immunity* 39(1):148–159.
39. Deng W, et al. (2012) Controlling long-range genomic interactions at a native locus by targeted tethering of a looping factor. *Cell* 149(6):1233–1244.

Supporting Information

Yashiro-Ohtani et al. 10.1073/pnas.1407079111

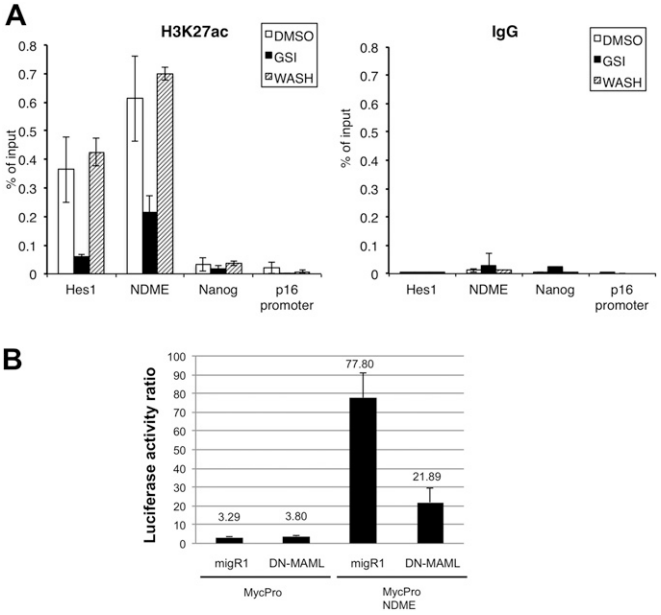

Fig. S1. Notch1 signaling regulates H3K27 acetylation of the murine *Myc* 3′ enhancer element (NDME). (*A*) T6E T-ALL cells treated with DMSO or 1 μM compound E for 16 h, or with compound E for 16 h followed by GSI washout and 4 h of additional incubation, were fixed and analyzed by local ChIP assay. ChIPs in *Left* were prepared with antibody specific for histone H3 acetylated at K27, whereas those in *Right* were prepared with a nonspecific Ig, as described (1). Data were obtained in triplicate in independent experiments; error bars correspond to the SEM. (*B*) Notch specifically regulates *NDME* activity. T6E cells were transfected with *Renilla* luciferase control (pRLTK), *Myc* promoter construct (*Myc*Pro) or the murine *Myc* enhancer reporter construct (*Myc*ProNDME) and either empty vector or a vector driving expression of the dominant-negative form of mastermind-like1 (DN-MAML).

1. Wang H, et al. (2014) NOTCH1-RBPJ complexes drive target gene expression through dynamic interactions with superenhancers. *Proc Natl Acad Sci USA* 111(2):705–710.

Myc 3′ enhancer alignment

```
mouse AAAGCTACTCTTAGAGGCAATTTGACAGAGCTGTCCTTTGAAACTGGCATTTTCTAAGTG 60
human AAAGGTGTTCTTAGTGGCAATTTAACAGAGCTGTCCTTTGAAAGTGGCATTTTCTAAGTA 60
      **** *  ****** ******** ****************** ***************

mouse TTCTTCTAAATTACAGTTGGGCCATAAATATGGCAGGTTAAACGGAGACAGCTGAGAAAT 120
human TTCTCCTAAATTGCAGTTGGGCCATAAATACAACAGGTTAAACTAAGGCAGCTGGGAAAT 120
      **** ******* ***************** ********** ** ****** *****

mouse GGTGTAGGTGAAAAATTACAAGGATGGGATCTTTCTCCTCTTCCACATGAAGATTTAATC 180
human TATATAGGTGAAAAATTACAAGGACGAGATCTTTCCACTCAAGCATGTAAAGATTTAATC 180
      * ******************* * ******** *** ** * ***********

                                                    RBPJ site B
mouse TGCCAGATTAAAAAACCCTGAACCTGGTGATTGTGTCAAGATAACAGCTTGGAGGATGCT 240
human TCCCAGGTTAAAAA-CCCAGAACACAGTGATTACTTTGAGATAACAGCTCAGAGGATGCT 239
      * **** ******* *** ****   ******   *  ***********  *********

          RBPJ site A
mouse CAGAGATGGGGTTCCCAGGGTGTTT-CAAGGGAT-GGGTCTGTGGCCTACAGAGGCAGGT 298
human CAGAGATGGGGTTCCCATGGTATTTTCTGGGGACCGGGTCTGTGGCCTGCAGAGGCAGGT 299
      ***************** *** *** *  ****  ************* ***********

mouse GTTTCTCAGTTGG-AGCACAGAGGAGTTCTTGGCACCAGCACTGGGCCAGCTGTGAGTTT 357
human GTTTCCCAGTGGGGAGCACAGAGGAGCCCTTTTCACCCGTATCAGGCCAGCTGTGAGCTT 359
      ***** **** ** ************  ***  **** * *   ************* **

mouse ATCTGTGGTATCTGGCTTTCAAAGTAGTGTTCCCTGCAGTCTGCCTAAAAGAAAGAGATG 417
human ATCTGTGGCATCTCGCTTTCAAGGAACGGTTCCCCAGGGTCTGCCTAGGAGAAAG----- 414
      ******** **** ******** * *  ******    *********  ******

mouse ATCAAGATGAACGAAGAGGTAATTGCACTGTACTCTACTCTGATGGGAAAAAGGGGGGAG 477
human -TT--GATGAACCACATGGGAACTGTACAGCATATTA-----ACAGGAAAAAAATGTAAA 466
       *   ******* *   ** ** ** ** * *   **     *  *******   *  *

mouse AATTATGAAAGAAAAATATATAT 500
human AATCATGAAACA---------- 478
      *** ****** *
```

Fig. S2. Sequence alignment of murine and human NDME elements.

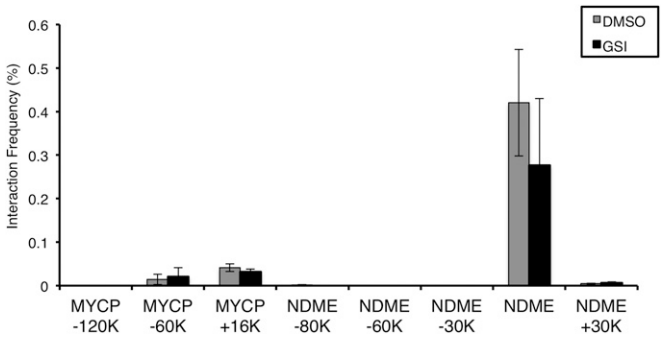

Fig. S3. Short-term Notch inhibition does not affect the interaction of the human *Myc* 3′ enhancer element (NDME) with the *Myc* promoter. Human CUTLL1 cells treated for 3 d with DMSO or 1 μM compound E were fixed and analyzed by 3C assay. The "probe" primer was located at the *Myc* promoter. Positions of other primers are shown in Fig. 5*C*. The 3C quantitative PCR (qPCR) products were quantified relative to the amounts of products generated with the same primer pairs, using a DNA substrate consisting of HindIII-digested, randomly ligated BAC DNA encompassing this region of the human genome. Data were obtained in triplicate in independent experiments; error bars correspond to the SEM.

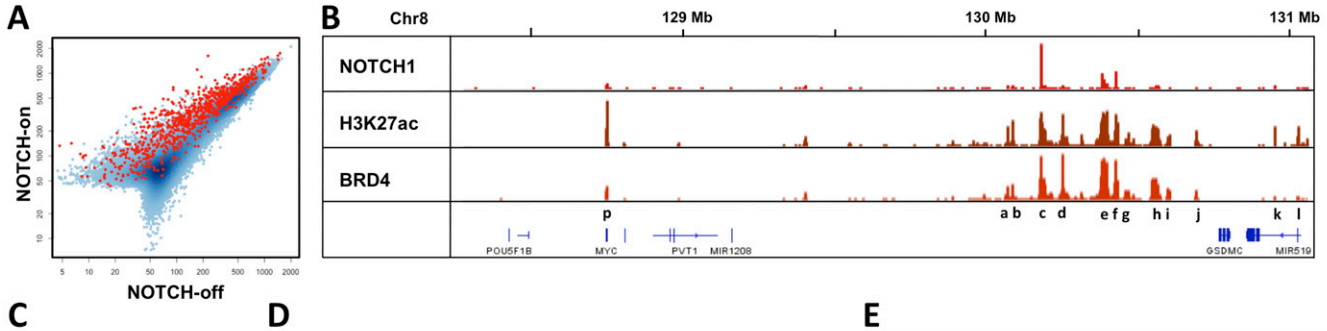

C

Annotation (chromosome 8)		
	start (kb)	end (kb)
p	128743.6	128754.8
a	130061.4	130076.8
b	130077.6	130104.0
c	130171.8	130220.4
d	130236.6	130275.0
e	130361.4	130410.8
f	130414.2	130438.0
g	130457.6	130482.2
h	130538	130574.6
i	130593	130609.4
j	130687.6	130710.8
k	130950.2	130953.4
l	131024.4	131030.8

D

H3K27ac						
	CUTLL		DND41		KOPTK-1	
	W4h/ GSI	P-value	GSI naïve/ resistant	P-value	GSI naïve/ resistant	P-value
p	1.44	9.0E-97	0.80	1	0.93	1
a	1.70	7.5E-106	5.27	0	4.59	0
b	1.61	1.1E-129	2.49	0	1.70	1E-147
c	1.71	0	8.63	0	6.93	0
d	1.78	0	7.26	0	8.92	0
e	1.91	0	2.10	5.5E-269	3.98	0
f	1.98	0	1.01	0.74	2.80	0
g	1.62	1.5E-98	0.77	1	1.35	7E-08
h	2.02	0	0.49	1	0.85	1
i	1.89	3.1E-128	0.35	1	0.66	1
j	2.45	0	0.33	1	0.76	1
k	0.96	1	0.63	1	0.95	1
l	1.01	0.6	0.82	1	0.69	1

E

BRD4				
	DND41		KOPTK-1	
	GSI naïve / resistant	P-value	GSI naïve/ resistant	P-value
p	0.89	1	1.27	5.5E-07
a	2.70	5.6E-29	7.90	2.4E-275
b	2.41	2.0E-34	10.60	0
c	5.96	0	22.63	0
d	3.90	2.6E-220	18.21	0
e	2.09	3.9E-50	4.98	0
f	1.30	7.9E-08	4.29	0
g	0.91	1	1.90	5.4E-19
h	0.71	1	1.22	4.6E-18
i	0.49	1	0.60	1
j	0.44	1	0.89	1
k	0.72	1	1.06	0.5
l	0.75	1	1.22	0.1

Fig. S4. Quantification of the effects of acute and chronic changes in Notch activation on chromatin landscapes in the Myc 3′ superenhancer region. (*A*) Scatterplot of H3K27ac ChIP-Seq read counts. Each dot represents an H3K27ac peak identified in CUTLL1 cells following GSI washout. ChIP-Seq reads within 600 bp of a peak summit were counted in the Notch-on and -off states. Red dots indicate peaks with dynamic Notch1 binding sites (described in ref. 1), and blue dots indicate peaks without dynamic Notch1 binding sties. (*B*) Chromatin landscapes in human CUTLL1 cells for Notch1, H3K27ac, and Brd4 are shown in the Notch-on state. (*C*) Genomic location of labeled peaks in *A*. (*D*) Quantification of changes in H3K27Ac peaks in CUTLL1 cells after 3 d of GSI treatment and 4 h after Notch1 reactivation by GSI washout (expressed as W4h/GSI) and in Notch-dependent (GSI naïve) and Notch-independent (GSI resistant) DND-41 and KOPT-K1 cells (expressed as GSI naïve/resistant). (*E*) Quantification of changes in Brd4 peaks in Notch-dependent (GSI naïve) and Notch-independent (GSI resistant) DND-41 and KOPT-K1 cells (expressed as GSI naïve/resistant).

1. Wang H, et al. (2014) NOTCH1-RBPJ complexes drive target gene expression through dynamic interactions with superenhancers. *Proc Natl Acad Sci USA* 111(2):705–710.

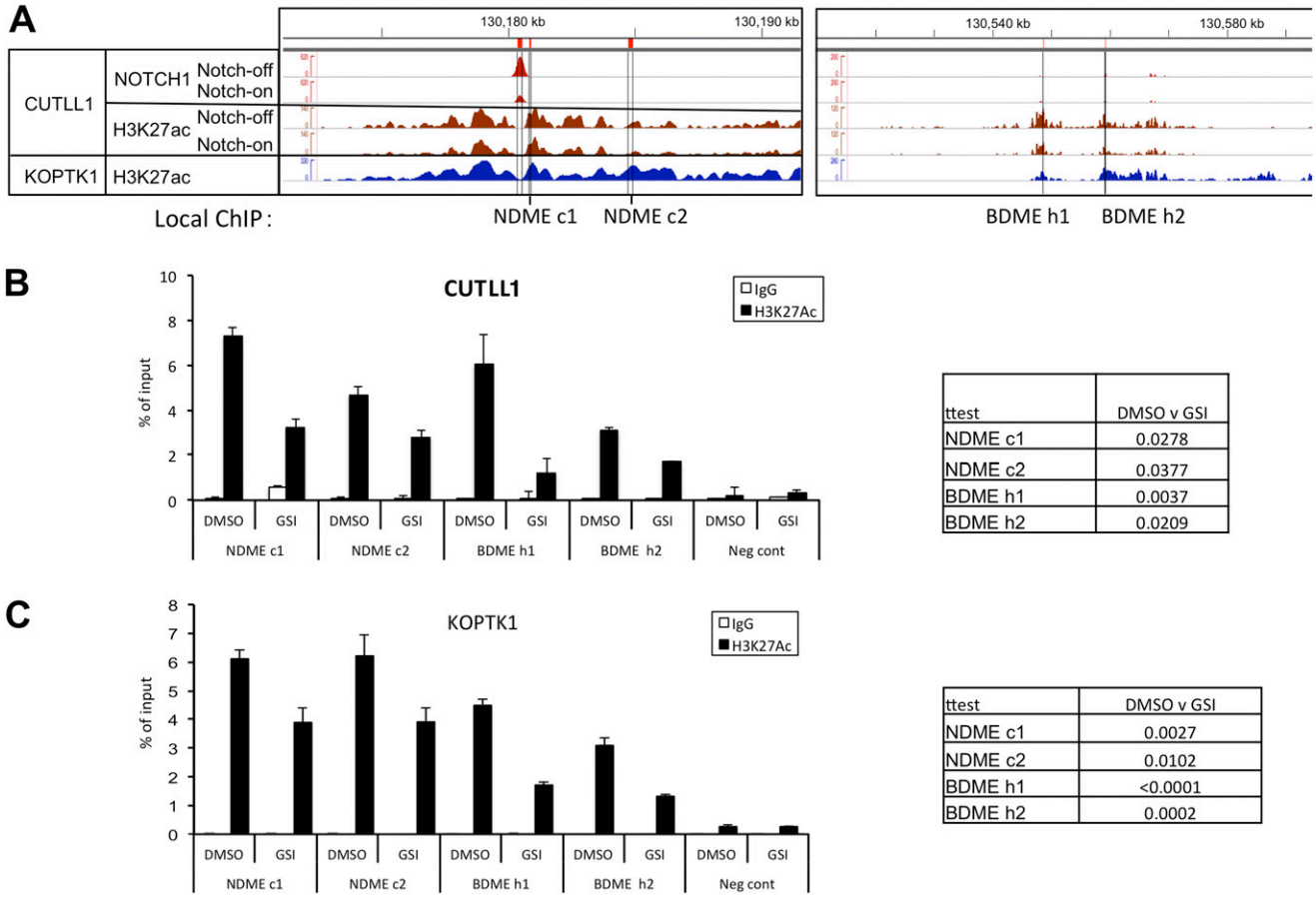

ttest	DMSO v GSI
NDME c1	0.0278
NDME c2	0.0377
BDME h1	0.0037
BDME h2	0.0209

ttest	DMSO v GSI
NDME c1	0.0027
NDME c2	0.0102
BDME h1	<0.0001
BDME h2	0.0002

Fig. S5. Notch1 signaling regulates H3K27 acetylation of the human NDME and BDME. (*A*) Position of primers used to perform H3K27ac local ChIP superimposed over Notch1 and H3K27ac ChIP-Seq data obtained from human CUTLL1 and KOPT-K1 T-ALL cells. (*B* and *C*) NDME c1 and NDME c2 denote two regions in peak c, and BDME h1 and BDME h2 denote two regions in peak h that were amplified using specific primer pairs. CUTLL1 and KOPT-K1 T-ALL cells treated with vehicle (DMSO) or 1 μM compound E (GSI) for 3 d were fixed and analyzed by local ChIP assays prepared with nonspecific IgG or antibody specific for K27-acetylated histone H3. Data were obtained in triplicate; error bars correspond to SD. *P* values were determined with Student *t* test.

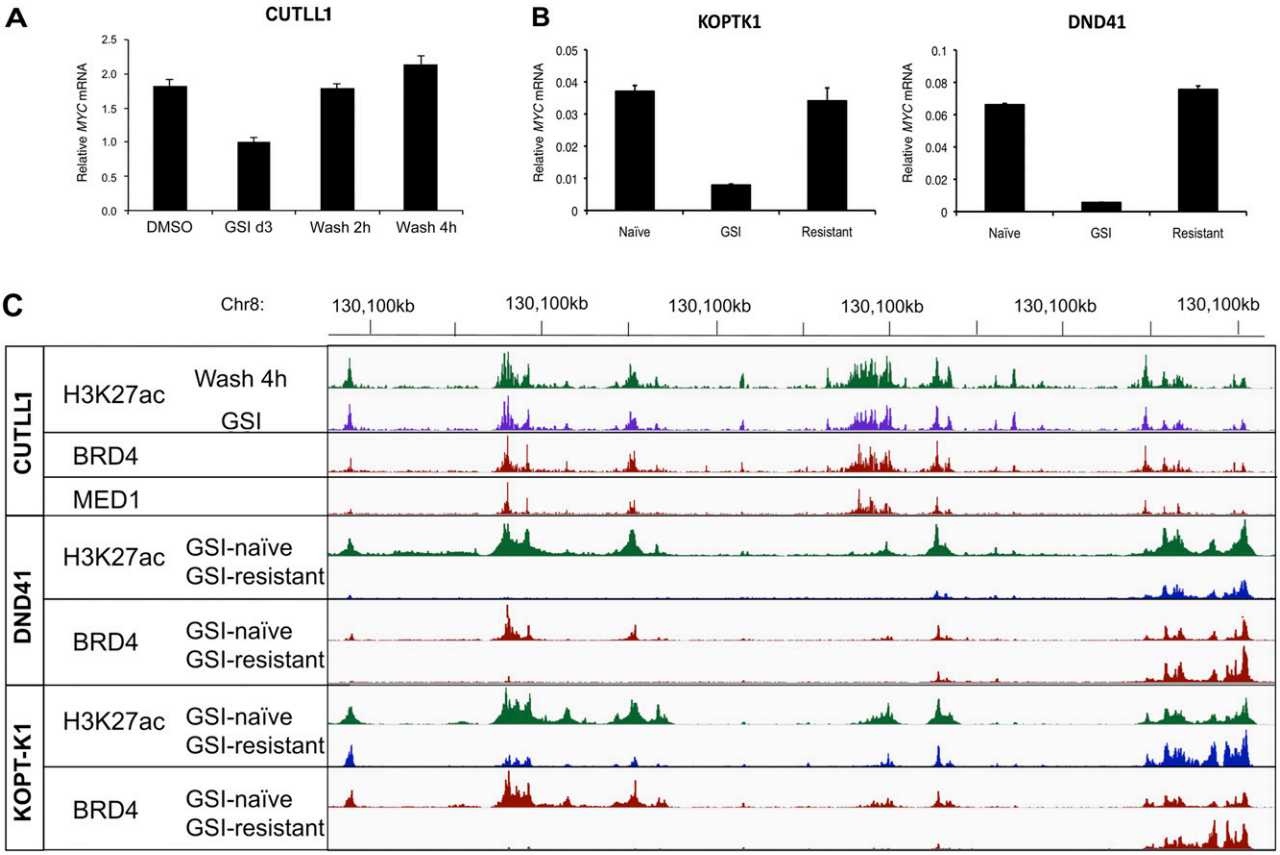

Fig. S6. Relative *Myc* mRNA expression in CUTLL1 cells following acute GSI blockade and washout and in GSI-sensitive and -resistant human KOPT-K1 and DND-41 cells. (*A*) *Myc* mRNA was quantified by qPCR in CUTLL1 cells incubated with vehicle, 1 μM compound E (GSI) for 3 d, or 1 μM compound E (GSI) for 3 d followed by 2 or 4 h of additional incubation after GSI washout. *Myc* expression was normalized to expression of the *Gapdh* housekeeping gene. (*B*) *Myc* expression in KOPT-K1 and DND-41 cells treated with vehicle for 3 d, GSI for 3 d, or selected for GSI resistant by long-term culture in GSI. *Myc* expression was normalized to expression of the *Gapdh* housekeeping gene. Data were obtained in triplicate in independent experiments; error bars correspond to the SEM. (*C*) Enlargement of the *Myc* 3′ enhancer cluster. The b–l peaks are defined in Fig. 5. See Fig. 5 for additional details.

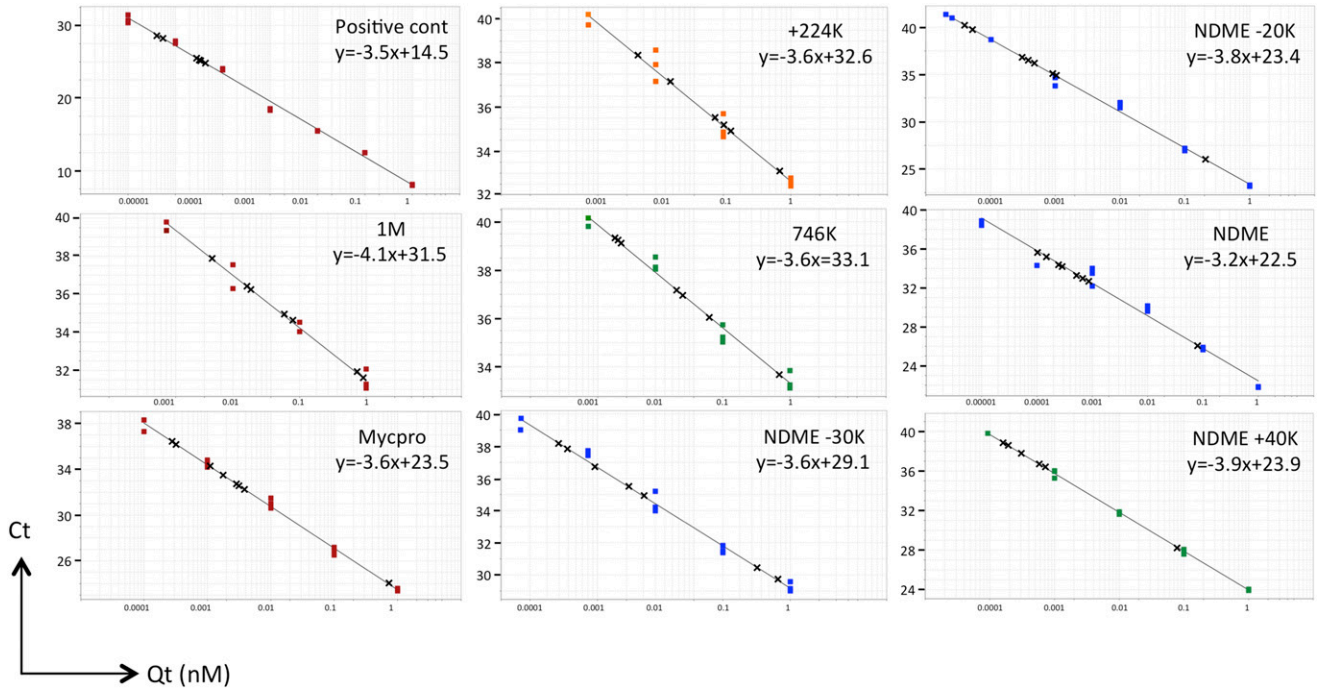

Fig. S7. Standard curves of qPCR for murine 3C experiments. Standard curves were prepared with serially diluted PCR DNA fragments (colored box). X shows Ct values from each PCR using 3C samples.

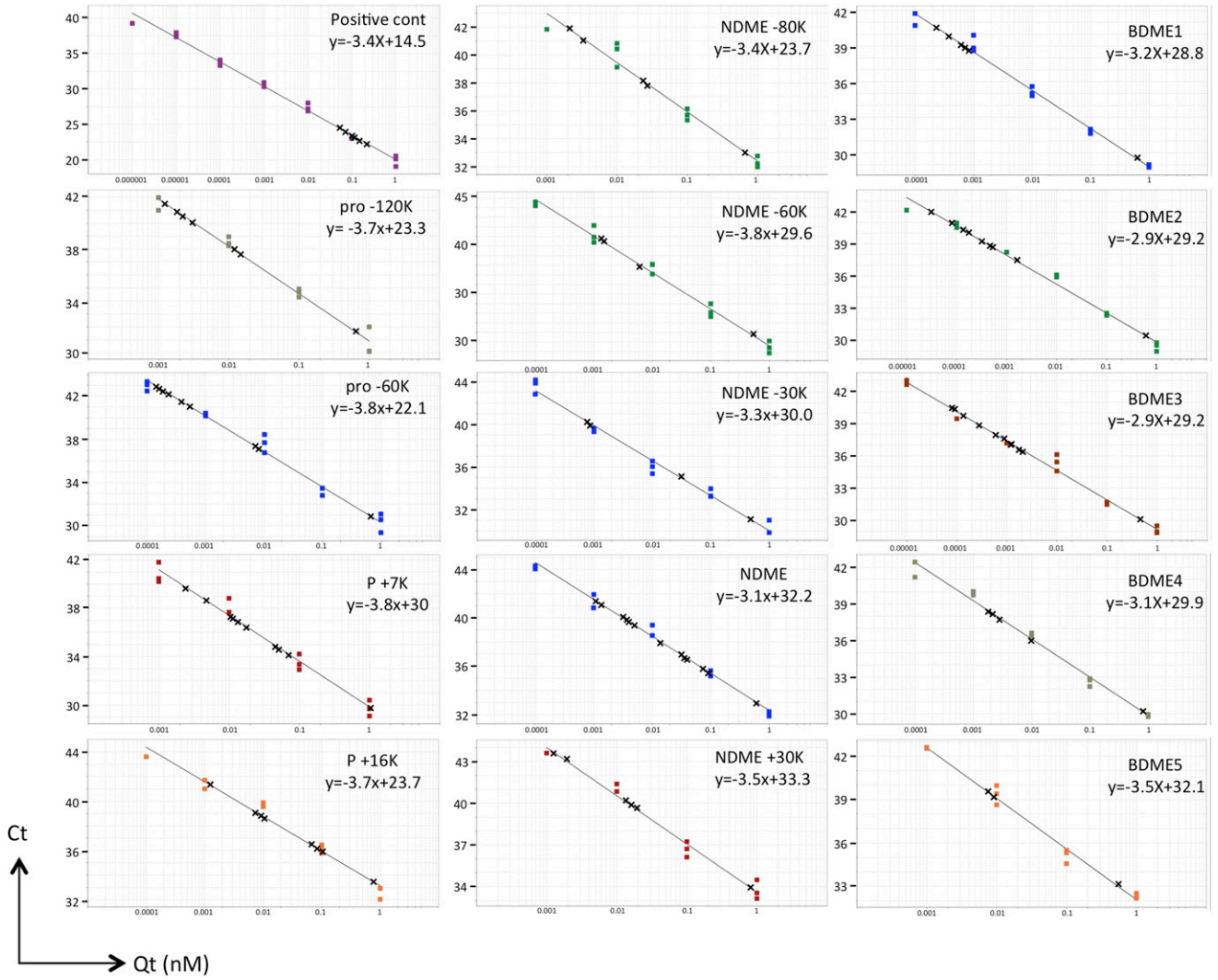

Fig. S8. Standard curves of qPCR for human 3C experiments. Standard curves were prepared with serially diluted PCR DNA fragments (colored box). X shows Ct values from each PCR using 3C samples.

Table S1. Primers used in these studies

	Forward	Reverse
ChIP primers		
Mouse Hes1 promoter	5′-TGCAGCGTCTCTGGGTTGTA-3′	5′-CCAGGACCAAGGAGAGAGGT-3′
Mouse Dtx1 intron3	5′-CGTGTCTCTTCCTCCCATTG-3′	5′-CCTGAGAGGAAGCGGTGT-3′
Mouse Myc enhancer	5′-ACCCTGAACCTGGTGATTGTG-3′	5′-CCACAGACCCATCCCTTGAA-3′
Mouse Nanog	5′-GGCTGCCTCTCCTCGCCCT-3′	5′-GTGCACACAGCTGGGCCTGA-3′
Human NDME c1	5′-GAGGCCCCCATTCATTACCC-3′	5′-CCAGGTAGGGGCATTACGTC-3′
Human NDME c2	5′-GCTGCCACATGCTGATGAAC-3′	5′-GCAGTTCTTCCTACGCTGGT-3′
Human BDME h1	5′-AGGAGCCCACCTTCTCATTT-3′	5′-ACATTGCAAGAGTGGCTGTG-3′
Human BDME h2	5′-AGGAAGTGGCTTTCACATGC-3′	5′-GCGTGCAAAAGAGAGAAACC-3′
human neg cont (+1M of *MYC*)	5′-AATGCTGGGCTTCCAAGGA-3′	5′-GACCTTGGTGACTGTTGAGGAAAC-3′
Cloning primers for pGL3		
Mouse Myc promoter	5′-GGTACCACGGTTTTCTTTATTCTAGGGTCT-3′	5′-GCTAGCCCCCAAATAGACAAAAATTCCCT-3′
Mouse Myc enhancer	5′-GGATCCACTGTTTGATTCTACCTCCCAAA-3′	5′-GGATCCTAGGCAGACTGCAGGGAAC-3′
Human MYC enhancer	5′-GGTACCGCTGTCCTTTGAAAGTGGCATT-3′	5′-GGTACCGCTGTACAGTTCCCATGTGGT-3′
Primers for 3C		
Mouse		
Myc probe	5′-FAM/AAGCCCTGCCCTTCAGGAGGC/TAMRA-3′	
Myc promoter F	5′-GTCCGACTCGCCTCACTCA-3′	
Myc control	5′-CCGCTCACTCCCTCTGTCTC-3′	
Myc promoter R	5′-CAAGGTTAGTGCCAAAGTCCATCT-3′	
Myc +224 K	5′-TGGTCTCCTGGTGCAGTTTG-3′	
Myc +746 K	5′-CAGCATGAATTATTTGACTTCTTGAAT-3′	
Human		
MYC probe	5′-FAM/CCCAGAAATGCTGGCTTTGCCA/TAMRA-3′	
MYC promoter F	5′-CTGCTACCTACCTCCAAAGCCTTA-3′	
MYC control R	5′-CCGCTCACTCCCTCTGTCTC-3′	
MYC promoter R	5′-GAGTGCATTCTCTCCACCACAGT-3′	
NDME -80K	5′-TCTCCAGAATGCTGTAAAGTAGACCA-3′	
NDME -60K	5′-GAATTCTATGTGCTCAGTGCCTTAAC-3′	
NDME -30K	5′-CTCCATTCCCTTCTGTATCTGCTATT-3′	
Mouse		
Myc+1M R	5′-AAGGCTCCCAGGTCAATGTG-3′	
NDME -30K	5′-TGTTTGCTTGCTTGCTTGATTT-3′	
NDME -20K	5′-CAAAGGCAGGATGGTTACTTTAGAA-3′	
NDME	5′-GTGTGTCACCGTGATTGTTCACT-3′	
NDME +40K	5′-TAAGGTAGACTTTCCATCTGACACAAA-3′	
Human		
NDME	5′-CTCCAGAGACAACAAGAGTGAGAAGAA-3′	
NDME +30K	5′-CAGCATTATCCATAGTAGCTCCAAACT-3′	
BDE E2 -23K	5′-ACCCCATAAGCACAGGCAAC-3′	
BDE E2	5′-GGTTCCAAAATCCGAGCTGA-3′	
BDE E3	5′-GCATGGCAGTGGTCACAGTT-3′	
BDE E4	5′-AAGAAGGTGGTTCTACCAAGAAAGG-3′	
BDE E4 +25K	5′-CCTGAAACCTGATTGCTCATGTAA-3′	
Myc+1M R	5′-AAGGCTCCCAGGTCAATGTG-3′	